Optimization of Methylene Blue Adsorption on Amphiprotic Bagasse Cellulose/TiO_2 Magnetic Aerogel by Response Surface Methodology

Sidan Li [a,b,c] Dong Xu,[a,b,c] Yuzhao Ma,[a,b,c] Xueyang Huang,[a,b,c] Yuehan Li,[a,b,c] Zheng Li,[a,b,c] and Yuan Yuan [a,b,c,*]

An amphoteric modification strategy was proposed to enhance the adsorption performance of biomass-based magnetic aerogels. Using sugarcane bagasse as the precursor, bagasse cellulose (BC) was extracted using a deep eutectic solvent at ambient temperature. Magnetic aerogels were fabricated by sequential cationization with 3-chloro-2-hydroxypropyltrimethylammonium chloride and anionization with 2-acrylamido-2-methylpropanesulfonic acid and amphiprotic BC/TiO_2 (AP-BC/TiO_2). These aerogels combined TiO_2 (a photocatalytic component) and Fe_3O_4 (a magnetic component) through an energy-efficient atmospheric pressure foaming process. The adsorption capacity for methylene blue (MB) was optimized using response surface methodology, with the mass concentrations of Fe_3O_4, AP-BC, and TiO_2 and initial concentration of MB as independent variables and the MB adsorption capacity as the response. A quadratic regression model was used to determine the optimal conditions. The AP-BC/TiO_2 magnetic aerogels exhibited an exceptional MB adsorption capacity of 1070 $mg \cdot g^{-1}$. Adsorption kinetics and isotherms were modeled, and the structural/physicochemical properties of the magnetic aerogels were characterized. The results confirmed the formation of a three-dimensional interconnected porous structure with uniform Fe_3O_4/TiO_2 loading and a saturation magnetization of 17.2 $emu \cdot g^{-1}$. This enabled rapid magnetic separation and confirmed the potential application of amphiprotic biomass-based magnetic aerogels as eco-friendly and cost-effective adsorbents for MB.

DOI: 10.15376/biores.21.4.9730-9746

Keywords: Amphiprotic cellulose; Bagasse; Magnetic aerogel; Methylene blue; Adsorption performance; Box–Behnken design

Contact information: a: College of Mechanical and Resource Engineering, Wuzhou University, Guangxi Wuzhou 543000, China; b: Guangxi Engineering Research Center of Comprehensive Utilization of Renewable Resources, Guangxi Wuzhou 543000, China; c: Guangxi University Engineering Research Center of Comprehensive Utilization of Renewable Resources, Guangxi Wuzhou 543000, China;
** Corresponding author: yuan__yuan2014@sina.com*

INTRODUCTION

Methylene blue (MB), a representative cationic synthetic weak-base dye, is widely applied in textile printing, dyeing, and pharmaceutical industries due to its superior color fastness, dyeing efficiency, and unique multifunctional properties (Su *et al.* 2024). Its positive charge is delocalized over the heterocyclic thiazine ring framework, rendering MB stable as a cationic species in aqueous media over the broad pH range of 3 to 10, including the pH = 8 condition used in this study. Accordingly, MB is classified as a typical cationic

organic water pollutant. However, the pollution caused by MB has become a critical environmental issue that demands urgent attention as annual global production of synthetic dyes exceeds 1 million tons and around 80% of dye-containing wastewater is discharged without adequate treatment (Liu *et al.* 2025). MB is characterized by high chemical stability and recalcitrance to biodegradation. MB can persist in aquatic ecosystems for prolonged periods, becoming a threat to fauna, disrupting biogeochemical cycles, and posing profound ecotoxicological threats. Even at trace concentrations ($\mu g \cdot L^{-1}$ level), positively charged MB can induce skin irritation, ocular impairment, and neurodegenerative disorders in humans through bioaccumulation in the food chain (Zeng *et al.* 2023). Accordingly, it is imperative to develop efficient strategies for the removal of cationic MB from alkaline wastewater (pH = 8) for environmental protection and public health safety.

Conventional wastewater treatment technologies for MB remediation, including membrane filtration, chemical precipitation, and heterogeneous photocatalysis, are often limited by exorbitant energy consumption, potential secondary contamination, and intricate operational protocols (Fu and Wang 2011; Gupta *et al.* 2013; Dai *et al.* 2021). By contrast, adsorption has emerged as the most promising strategy due to its simple operation, cost-effectiveness, and high removal efficiency (Fang *et al.* 2025; Gong *et al.* 2025). Traditional adsorbents such as activated carbon, sponge, zeolite, microbial-based adsorbents, and unmodified biomass typically exhibit limited MB adsorption capacities (usually 200 to 600 $mg \cdot g^{-1}$) and poor recyclability, significantly hindering their large-scale industrial deployment (Chen *et al.* 2016).

Another viable option for adsorption is bioadsorbents obtained from agricultural wastes. These adsorbents offer numerous benefits such as cost-effectiveness, ready accessibility, and a high adsorption capacity. Nonetheless, most reported biomass-based adsorbents lack structural optimization and functional integration, failing to meet the requirements for high-performance sustainable treatment of alkaline cationic dye wastewater. The development of eco-friendly, recyclable, and ultra-high-capacity adsorbents remains an urgent scientific and technological challenge. Organic dye contaminants such as positively charged MB feature strong environmental persistence due to their stable chemical structures and resistance to degradation, and they show high toxicity including acute cytotoxicity, chronic endocrine disruption, genotoxicity, and carcinogenicity, posing persistent risks to aquatic ecosystems and human health through bioaccumulation and food chain magnification (Mubarak *et al.* 2024).

Lignocellulosic biomass's abundance, renewability, low cost, and inherent biodegradability, in particular agricultural residues such as sugarcane bagasse, has garnered interest as a potential raw material for fabricating adsorbents (Sen *et al.* 2022; Xiao *et al.* 2023; Chen *et al.* 2024). Sugarcane bagasse, a major byproduct of the sugar industry, contains high levels of cellulose (32 to 45%), hemicellulose (20 to 30%), and lignin (15 to 25%), providing a robust porous scaffold for constructing advanced adsorbent materials (Chen *et al.* 2016). Biomass aerogels, distinguished by their three-dimensional (3D) interconnected porous architecture, ultra-high specific surface area, and extremely low bulk density, have emerged as ideal candidates for adsorbing pollutants (El-Sawaf *et al.* 2024a; Su *et al.* 2024). They are synthesized *via* lignocellulose dissolution, gelation, and drying processes. However, these energy-intensive processes often require elevated temperatures (>100 °C) or traditional solvent systems containing toxic reagents (*e.g.*, DMSO/LiCl), leading to environmental contamination and exorbitant energy expenditure (Gong *et al.* 2025).

Deep eutectic solvents (DESs), as green, eco-friendly, and recyclable alternatives to conventional organic solvents, have low toxicity, facile synthesis, tunable physicochemical properties, and excellent biocompatibility that revolutionized the extraction of cellulose and preparation of aerogels (Almeida *et al.* 2023; Nie *et al.* 2025; Tong *et al.* 2025). Gong *et al.* (2025) overcame the limitations of high-temperature processes through a room-temperature DES system ($ZnCl_2/H_3PO_4/(NH_4)_2HPO_4$/water) for cellulose nanofiber extraction with a yield of ~90%.

To further enhance the affinity of biomass aerogels for positively charged cationic MB, amphoteric modification has been established as a viable approach (Xiong *et al.* 2020; Su *et al.* 2024). Amphoteric cellulose, functionalized with anionic (*e.g.*, sulfonic acid) groups, can enhance the adsorption of cationic MB through multiple interfacial interaction mechanisms, including electrostatic attraction, hydrogen bonding, and ion exchange (Qiu *et al.* 2022). Typically, cationization is achieved using 3-chloro-2-hydroxypropyl-trimethylammonium chloride (CTA), while anionization can be accomplished with 2-acrylamido-2-methylpropanesulfonic acid (AMPS). For instance, Xiong *et al.* (2020) fabricated amphiprotic cellulose-mediated graphene oxide magnetic aerogels with an MB adsorption capacity of 346 $mg \cdot g^{-1}$. The amphiprotic characteristic of the magnetic aerogel arises from amphiprotic microcrystalline cellulose (AP-MCC) rather than iron-based sites. Fe_3O_4 only provides magnetic recyclability and does not participate in protonation or acid–base interactions. AP-MCC is covalently modified with quaternary ammonium cationic sites and sulfonate anionic sites. Quaternary ammonium groups act as basic sites that easily accept protons and carry stable positive charges in acidic water, while sulfonate groups dissociate to form negative charges under alkaline conditions (pH = 8). This pH-responsive surface charge switch enables the amphiprotic adsorbent to generate strong electrostatic attraction toward positively charged MB at alkaline pH.

However, existing research still encounters critical challenges: (1) Amphoteric modification processes often involve harsh reaction conditions (such as, high temperature and strong acid/base), resulting in reduced cellulose crystallinity and intense structural damage; (2) The preparation of magnetic aerogel predominantly relies on freeze-drying, which is energy-intensive and cost-prohibitive for large-scale production; (3) Optimization of process parameters for aerogel synthesis and adsorption is largely based on empirical methods, lacking systematic statistical approaches (such as, response surface methodology (RSM)) to maximize performance; and (4) The integration of adsorption and photocatalytic degradation for synergistic pollutant elimination in magnetic aerogels remains underexplored, limiting their potential applications in complex wastewater treatment scenarios (El-Sawaf *et al.* 2024b).

To bridge these gaps, the current study proposes a circular bioeconomy-aligned strategy for magnetic aerogels with ultrahigh adsorption capacity for positively charged MB under pH = 8 alkaline conditions. Briefly, ternary DES ($ZnCl_2/H_3PO_4/NH_4H_2PO_4$) was used to extract BC at room temperature, allowing for selective delignification while preserving crystallinity. The BC was then modified *via* a mild stepwise CTA/AMPS process to introduce dual functional groups. Atmospheric pressure foaming with polyvinyl alcohol/chitosan blend (PVA/CS) was used as a low-energy alternative to freeze-drying. Parameter optimization was conducted using Box–Behnken design (BBD)-RSM, and an integration of adsorption, photocatalysis, and magnetic separation was implemented. Fourier-transform infrared (FTIR) spectroscopy, X-ray diffraction (XRD) analysis, scanning electron microscopy-energy-dispersive X-ray spectrometry (SEM-EDS), and

vibrating sample magnetometry (VSM) techniques were employed to characterize the samples. The adsorption mechanism was also considered.

EXPERIMENTAL

Materials

Bagasse obtained from a local factory in Wuzhou, China was processed into smaller particles using a flaker (FW-100 high-speed shredder, Changzhou, China). The initial moisture content is 12%. The obtained particles were dried to a moisture content of 5% and separated through a 60-mesh sieve. Zinc chloride ($ZnCl_2$, ≥98.0%), phosphoric acid (H_3PO_4, purity 85%), ammonium dihydrogen phosphate ($NH_4H_2PO_4$, ≥98.0%), PVA (Mw = ~77,000 g·mol^{-1}, hydrolyzed: >99%)), CS (deacetylation >95%), acetic acid (CH_3COOH), sodium dodecyl sulfate (SDS), titanium dioxide (TiO_2), and ferroferric oxide (Fe_3O_4) were purchased from Shanghai Macklin Biochemical Technology Co., Ltd., China. CTA (CAS Number 3327-22-8), AMPS (CAS Number 15214-89-8), and ammonium ceric nitrate ($Ce(NH_4)_2(NO_3)_6$, CAS Number 16774-21-3) were procured from Shanghai Aladdin Biochemical Technology Co., Ltd., China.

Synthesis of AP-BC

The BC was extracted as follows. First, the mesocarp layer, obtained after removing bagasse, was mixed with a ternary DES ($ZnCl_2$/H_3PO_4/$NH_4H_2PO_4$ with a molar ratio of 1:0.3:1) at a solid-to-liquid ratio of 1:20 (g:mL) under vigorous mechanical stirring at room temperature. The components were allowed to swell for 12 h and then sheared at 3500 rpm using a high-speed mixer (IKA T25, Germany) for 30 min. After the reaction, the mixture was filtered. The solid product was soaked in deionized water for 24 h, rinsed three times with distilled water, and dried at 60 °C to constant weight to obtain BC.

The amphoteric modification procedure utilized in this study was based on previously published methods (Xiong *et al.* 2020) with necessary improvements. First, BC (5 g) was dispersed in ethanol. Then, NaOH (5 mL, 100 g·L^{-1}) and CTA (10.0 g) as the cationic monomer were added dropwise in succession to the mixture, followed by continuous stirring at 45 °C for 3 h to conduct the quaternization process (Ragab *et al.*, 2024a). The product was filtered, washed with methanol and ethanol, and dried to obtain CTA-BC. Next, it was dispersed in deionized water by stirring under nitrogen atmosphere at room temperature for 10 min. $Ce(NH_4)_2(NO_3)_6$ (6.0 g) was added and stirred for 30 min. AMPS (6.0 g) as the anionic monomer was added to the mixture and stirred for 1.0 h. The final mixture was allowed to react at 50 °C for 1.0 h to carry out the sulfonation process. Thereafter, cellulose was filtered, washed successively with deionized water, acetone, and diethyl ether, and dried at 60 ℃ for 2 h to obtain the AP-BC.

Preparation of Aerogel

To prepare the PVA aqueous solution, 2 g of PVA powder was mixed with deionized water at 1:8 (g:mL). The mixture was fully dissolved under constant stirring at 500 rpm in a thermostatted water bath at 90 °C. Next, CS (0.3 g) was dissolved in 2% acetic acid solution (50 mL) and the contents were stirred for 30 min to prepare a CS solution The AP-BC suspension, PVA solution, and CS solution were mixed, followed by the addition of SDS (0.6 g·L^{-1}), TiO_2 (1 g·L^{-1}), and Fe_3O_4 (4 g·L^{-1}). The mixture was stirred

at 3000 r·min^{-1} for 15 min for foaming, then poured into a 60 mm × 60 mm square mold that stood at room temperature for 15 min, and finally dried at 60 °C to obtain magnetic aerogel.

FTIR Spectroscopy and XRD Analyses

FTIR spectroscopy (Thermo Fisher Scientific, Waltham, MA, USA) was employed to analyze changes in functional groups of the samples. The KBr tablet method was employed, and powder samples were used. FTIR spectra were recorded from 4000 to 400 cm^{-1} at a resolution of 4 cm^{-1}, with a scanning time of 40. XRD analysis was carried out to characterize the crystal structure and relative crystallinity of the samples. The scanning range was 10° to 40° at a scanning speed of 5° min^{-1}, and the step distance was 0.02°. The crystallinity index of the sample was calculated in accordance with a previous study (Segal *et al.* 1959).

SEM-EDS Analysis

SEM images were recorded on a Sirion 200 instrument (FEI, Hillsboro, The Netherlands) to evaluate the morphological changes on the CS surface subjected to different pretreatments. The samples were sprayed with gold to increase their conductivity. The high-vacuum mode was adopted for tests, SEM images were recorded at a beam voltage of 12.5 kV, and the elemental composition was analyzed.

Magnetic Performance Analysis

The magnetic performance of the as-prepared biomass-based magnetic aerogel was systematically evaluated by VSM (Lake Shore 7410) at ambient temperatures (25±1 °C). The magnetic hysteresis loops (M–H loops) were recorded by scanning the applied magnetic field in the range of −30,000 to +30,000 Oe (1 Oe = 79.577 A·m^{-1}) with a scanning rate of 100 Oe·s^{-1}.

Adsorption Experiment

The batch adsorption with gentle agitation was employed to conduct adsorption experiments on MB solutions with concentrations of 240 to 360 mg·L^{-1} (pH = 8, 30 °C) for 120 min. All adsorption experiments under each condition were conducted in triplicate. The residual concentrations of the solutions were determined using an ultraviolet–visible (UV–vis) spectrophotometer at the characteristic wavelengths of 664 nm for cationic MB. The MB adsorption capacity was calculated by weight measurements.

Table 1. Experimental Design of Coded Factors and Results of BBD for MB Adsorption Capacity on AP-BC/TiO_2 Magnetic Aerogel

Coded	Factors		Range and Levels		
			Low (-1)	Medium (0)	High (1)
A	Mass concentration of Fe_3O_4 (g/L)		3	4	5
B	Mass concentration of AP-BC (g/L)		1	3	5
C	Mass concentration of TiO_2 (g/L)		1	2	3
D	Initial concentration of MB (mg/L)		240	300	360
Run	Factors				MB adsorption capacity (mg/g)
	A	B	C	D	
1	-1	0	1	0	1037.75±5.8
2	0	0	0	0	1065.43±6.4
3	1	-1	0	0	998.44±4.3

Coded	Factors		Range and Levels		
			Low (-1)	Medium (0)	High (1)
4	-1	-1	0	0	1026.92±5.6
5	0	0	-1	1	1077.40±6.2
6	1	1	0	0	1044.36±7.4
7	0	1	1	0	1069.71±6.3
8	0	0	-1	-1	1060.12±4.8
9	0	0	1	1	1076.92±6.0
10	-1	0	0	1	1043.71±5.4
11	0	-1	-1	0	1055.92±6.8
12	-1	1	0	0	1043.78±4.7
13	0	1	-1	0	1042.36±7.1
14	0	0	0	0	1059.81±5.5
15	1	0	0	-1	948.95±6.4
16	0	-1	0	-1	983.07±4.8
17	1	0	1	0	1027.54±7.2
18	0	1	0	-1	966.93±4.3
19	0	0	0	0	1070.52±4.0
20	0	0	1	-1	1051.20±5.9
21	0	0	0	0	1057.56±7.2
22	0	-1	0	1	1030.70±4.3
23	0	1	0	1	1049.10±5.4
24	-1	0	-1	0	1066.34±6.0
25	0	-1	1	0	1015.66±6.3
26	1	0	-1	0	1033.32±4.5
27	0	0	0	0	1060.97±7.8
28	1	0	0	1	1018.93±6.4
29	-1	0	0	-1	1003.12±4.5

Experimental Design

A BBD with four independent parameters and three levels was adopted using Design-Expert 8.0.6 software (Stat-Ease Inc., Minneapolis, USA). In total, 29 experiments were conducted at a central point to determine the variables that influence MB adsorption capacity. This method allows the establishment of statistical relationships between the experimental variables and response variables to describe the response surface and elucidate optimal manufacturing conditions. These features should, in turn, predict the optimal board properties. Table 1 lists the design matrix and adsorption capacities of the obtained AP-BC/TiO_2 magnetic aerogel.

The four critical parameters that affected the MB adsorption capacity of the AP-BC/TiO_2 magnetic aerogel included mass concentration of Fe_3O_4 (A), mass concentration of AP-BC (B), mass concentration of TiO_2 (C), and initial concentration of MB (D). These parameters were selected as independent variables based on preliminary experiments. An analysis of variance (ANOVA) was performed for the response at a confidence level of 95%. All data were expressed using the average of three replicates and their coefficient of variations (CVs). The CV observations for the samples (AP-BC/TiO_2 magnetic aerogel) were consistent with those of the control (BC/TiO_2 magnetic aerogel).

RESULTS AND DISCUSSION

Data Analysis and Regression Models

The ANOVA p-values for Q_e are presented in Table 2. All p-values below 0.05 revealed significant model terms, while values above 0.05 indicated insignificant model terms (Alslaibi *et al.* 2013). Moreover, p-values below 0.0001 indicated that the model for the MB adsorption capacity was statistically significant, and there was a 0.01% chance that such values could occur due to noise. In this case, A, B, C, D, AB, BC, A^2, B^2, C^2, and D^2 were significant model terms. The regression equation is as follows:

$$\text{Adsorption capacity of MB} = 1062.86 - 8.17A + 12.63B - 6.97C + 14.03D + 26.76AB + 10.16BC - 32.13A^2 - 25.65B^2 + 11.89C^2 - 12.13D^2 \quad (1)$$

The models were a good fit, with an overall R^2 value of 0.9621. The predicted R^2 value (0.8918) agreed with the adjusted R^2 value (0.9410). Values of adequate precision greater than 4 are desirable (Muthukumar *et al.* 2003). The Lack of Fit F-value of 0.2647 suggested that the model was non-significant. The low coefficient of variance (C.V.% = 0.66) confirmed the accuracy and reliability of the experimental values in the regression model.

Table 2. Analysis of Variables for Parameters and their Interactions

Source	Sum of Squares	df	Mean Square	F-value	P-value
Model	21518.6	14	2151.869	45.69258	< 0.0001
A	801.6405	1	801.6405	17.02203	0.0006
B	1914.455	1	1914.455	40.65154	<0.0001
C	582.9708	1	582.9708	12.3788	0.0025
D	2362.371	1	2362.371	50.16258	<0.0001
AB	2865.461	1	2865.461	60.84518	<0.0001
BC	413.1056	1	413.1056	8.771883	0.0084
A^2	6695.996	1	6695.996	142.1828	<0.0001
B^2	4267.827	1	4267.827	90.62302	<0.0001
C^2	916.3271	1	916.3271	19.45728	0.0003
D^2	954.5064	1	954.5064	20.26798	0.0003
Residual	847.6973	14	47.09429		
Lack of fit	741.4522	10	52.96087	1.993913	0.2647^{ns}
Pure error	106.2451	4	26.56127		
Cor total	22366.29	28			

^{ns} Not significant

Response Surface Interaction Analysis

Figure 1 displays the 3D response surface and contour plots for MB adsorption capacity. The 3D response surface plot and the 2D response contour plot provide a visual interpretation of the interaction between two independent variables. For instance, the 3D response surface diagram exhibits interaction between independent variables and response variables. Conversely, the 2D response contour map can explain the interaction between independent variables and reflect the importance of this interaction. The circular response contour plot demonstrates that the interaction between the corresponding variables is

negligible, whereas the elliptic response contour plot shows significant interaction between the corresponding variables (Yuan *et al.* 2019).

As depicted in Fig. 1, the significant interaction combinations AB and BC were selected to analyze their interactive effects on the MB adsorption capacity. The interaction effect between the mass concentration of Fe_3O_4 (A) and the mass concentration of AP-BC (B) was greater than that between the mass concentration of AP-BC (B) and the mass concentration of TiO_2 (C). Figure 1a illustrates that for the fixed mass concentration of AP-BC, the adsorption capacity first increased and then decreased with increasing mass concentration of Fe_3O_4. For the fixed mass concentration of Fe_3O_4, the effect of AP-BC mass concentration on the MB adsorption capacity also first increased and then decreased. The mass concentrations of AP-BC and Fe_3O_4 significantly impacted the adsorption capacity. The optimal adsorption effect of this response model occurred when the mass concentration of AP-BC was between 2.5 and 4.5 $g \cdot L^{-1}$, and the mass concentration of Fe_3O_4 was in the 3.5 to 4.5 $g \cdot L^{-1}$ range. Figure 1b demonstrates that the effect of the mass concentration of AP-BC on the MB adsorption capacity first increased, then decreased when the mass concentration of TiO_2 was fixed. The adsorption effect of this response model improved when the mass concentration of AP-BC ranged from 2.5 to 3.5 $g \cdot L^{-1}$, and TiO_2 was 1.0 to 1.5 $g \cdot L^{-1}$.

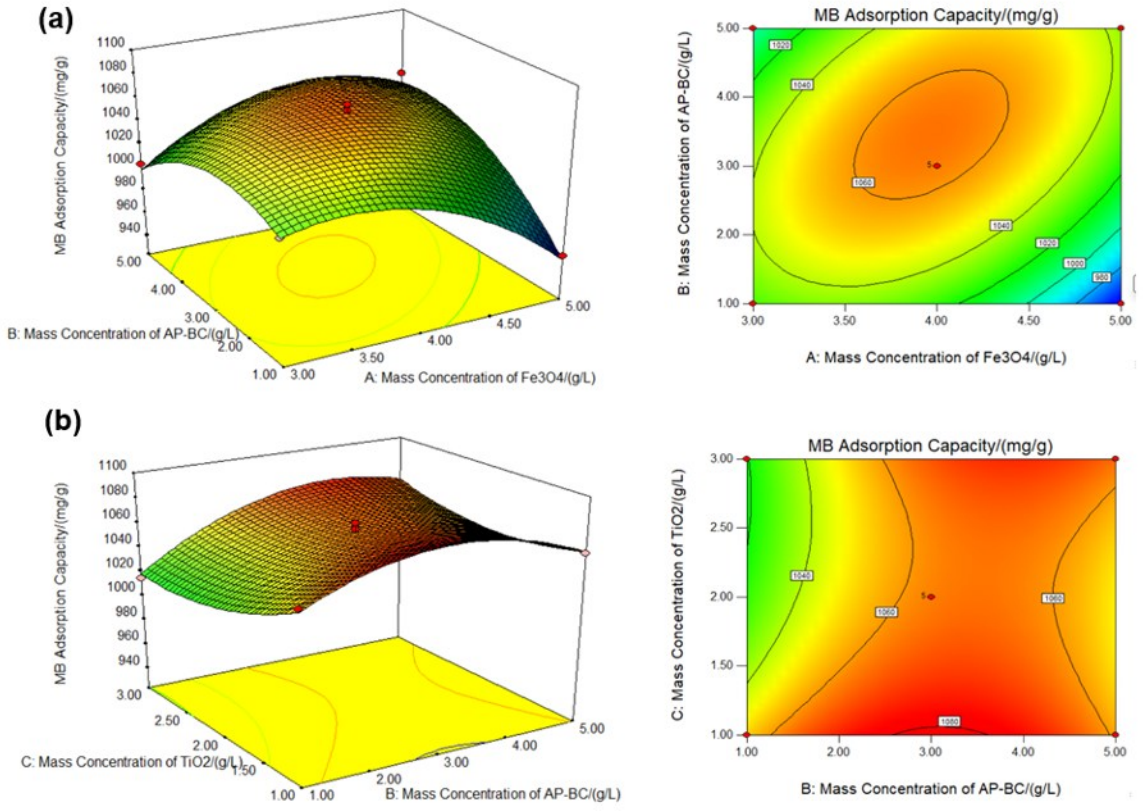

Fig. 1. Response surface plots and response contour plots showing the interaction effect of AB and BC on the MB adsorption capacity

Optimization and Verification Experiment

Following the optimization analysis, validation experiments were conducted using the same method under optimal conditions: Fe_3O_4 mass concentration of 3.96 g·L^{-1}; AP-BC (B) mass concentration of 3.06 g·L^{-1}; TiO_2 mass concentration of 1.08 g·L^{-1}; and initial MB concentration of 300.01 mg·L^{-1}. These conditions resulted in a predicted MB adsorption capacity of 1080 mg·g^{-1}. The experiment was optimized for convenience by adjusting the process parameters as follows: Fe_3O_4 mass concentration of 4.0 g·L^{-1}; AP-BC (B) mass concentration of 3.0 g·L^{-1}; TiO_2 mass concentration of 1.0 g·L^{-1}; and initial MB concentration of 300 mg·L^{-1}. The observed MB adsorption capacity under these conditions was 1074.6±5.6 mg·g^{-1}, demonstrating the model's high reliability and good reproducibility of the MB adsorption capacity. This is in contrast to BC/TiO_2 magnetic aerogels' low adsorption capacity of MB (only 208.9±3.7 mg·g^{-1}), indicating that this model is suitable for optimizing the adsorption capacity of MB.

Synthesis and Characterization

FTIR analysis

The FTIR spectra of native bagasse, BC, and AP-BC are shown in Fig. 2. The bands of raw bagasse at 1,605, 1,515, and 835 cm^{-1} were associated with the ring breathing combined with C–O stretching, aromatic skeletal vibrations, and aromatic C–H out-of-plane vibration in lignin (Nuopponen *et al.* 2005). Absorbances at 1,375 and 1,240 cm^{-1} were attributed to the bending of C–H and the antisymmetric stretching of C–O in the acetyl group of hemicelluloses. These bands in BC were weakened, suggesting that the DES treatment removed some of the lignin and hemicellulose from the BC. The FTIR spectrum of BC showed the disappearance of the peak at 1,238 cm^{-1}, suggesting that CTA had been grafted to the C6 site of BC to substitute the primary hydroxyl group. The peaks at l,650 and 1,551 cm^{-1} in AP-BC were attributed to the stretching vibration of amide I and the bending vibration of amide II (Xiong *et al.* 2020). This suggests that the amide group was introduced in BC after grafting AMPS, confirming the successful incorporation of both CTA and AMPS monomers in BC to produce the desired AP-BC (Ragab *et al.*, 2024b).

The pH-responsive surface charge conversion behavior of AP-BC plays a decisive role in its excellent adsorption performance toward positively charged MB under the experimental condition of pH = 8. The amphiprotic structure endows AP-BC with reversible surface charge switching properties: in acidic environments, protonated quaternary ammonium groups dominate and render the aerogel positively charged. Sulfonate groups are fully dissociated across the studied pH range, and alkaline conditions yield a net negative surface charge on the aerogel. At the fixed experimental pH = 8 adopted in this study, the AP-BC/TiO_2 aerogel surface is rich in dissociated negative charges, which produces strong electrostatic attraction toward positively charged cationic MB molecules. This electrostatic interaction serves as the dominant driving force for efficient MB capture, completely matching the cationic characteristics of MB dye in alkaline aqueous solution (Elfiky *et al.* 2024).

The adsorption of MB onto the AP-BC/TiO_2 aerogel is predominantly governed by chemisorption and strong electrostatic interactions under the optimal experimental condition of pH = 8. At this alkaline pH, the AP-BC/TiO_2 aerogel presents a negatively charged surface, which effectively captures positively charged cationic MB molecules *via* coulombic attraction as the dominant adsorption force. In addition, abundant hydroxyl and carboxyl functional groups on the aerogel skeleton form hydrogen bonds with MB molecules. Weak π–π stacking may also form between aromatic moieties, contributing

auxiliary adsorption interaction. The well-developed hierarchical porous structure and high specific surface area supply sufficient accessible active sites and promote intra-particle diffusion, facilitating efficient mass transfer (Nassar *et al.* 2025). The adsorption process was well described by the pseudo-second-order kinetic model and Freundlich isotherm. Consistent with the conclusions of Hubbe *et al*. (2019), the good fit to the pseudo-second-order model implies that the adsorption rate is governed by intraparticle diffusion through the aerogel's porous framework, while the Freundlich isotherm confirms that adsorption takes place on a chemically heterogeneous surface (Ramzi *et al.* 2016)

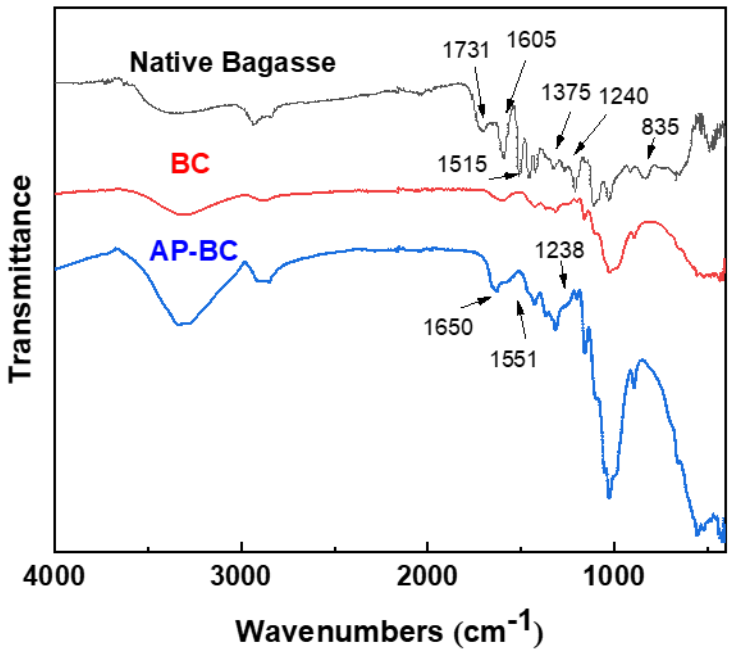

Fig. 2. FTIR spectra of native bagasse, BC, and AP-BC

XRD analysis

XRD patterns of native bagasse, BC, and AP-BC are shown in Fig. 3. Figure 3a illustrates that the diffraction peaks of native bagasse at 15.8°, 22.2°, and 34.5° were assigned to Miller indices of (110), (200), and (004) of cellulose I pattern (Salem *et al.* 2023). In particular, the diffraction intensity of BC peaks increased, with the Crl values rising from 43.2% in native bagasse to 54.8% in BC (Fig. 3b). This indicated that the acid treatment effectively eliminated the amorphous region and enhanced the crystallinity of BC. As a result, a notable decrease in crystallinity was observed in AP-BC (37.4%) compared to BC (54.8%). This means that the amphoteric modification process disrupted some crystalline regions in BC, leading to an expanded cellulose microstructure.

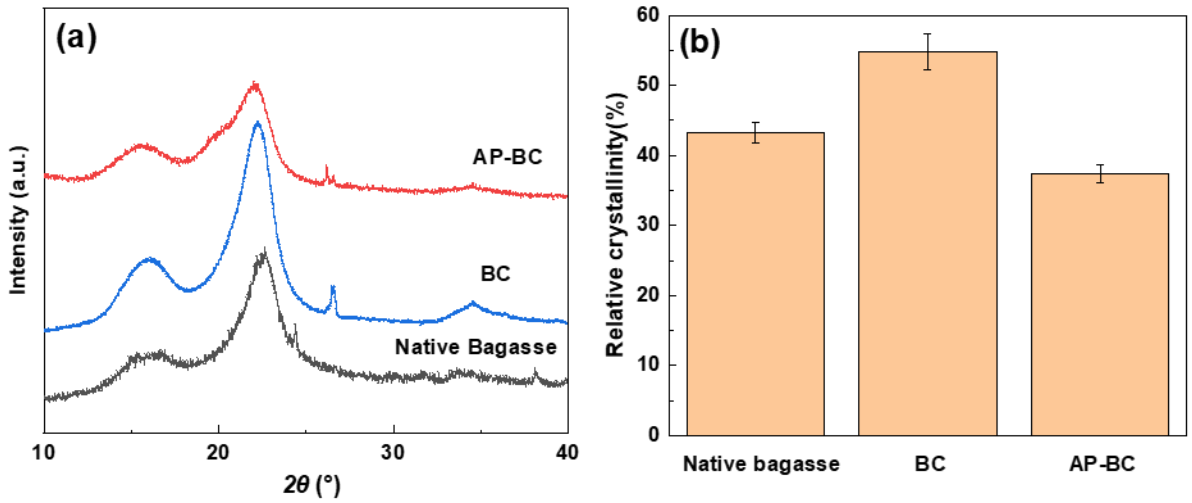

Fig. 3. (a) XRD patterns and (b) relative crystallinity of native bagasse, BC, and AP-BC

SEM-EDS analysis

Figure 4 shows the SEM images and EDS spectra of the AP-BC/TiO_2 magnetic aerogel. The figures demonstrate that the AP-BC/TiO_2 magnetic aerogels exhibited a 3D interconnected porous network structure, with Fe_3O_4 and TiO_2 particles loaded on the pore wall surfaces. The AP-BC skeletons were sufficiently and organically integrated to produce a clearly defined 3D multichannel structure with a specific orientation. The EDS elemental analysis confirmed that the magnetic aerogels contained 27.2% Ti and 17.9% Fe, supporting the presence of Fe_3O_4 and TiO_2. This unique 3D interconnected porous structure plays a crucial role in enhancing adsorption performance.

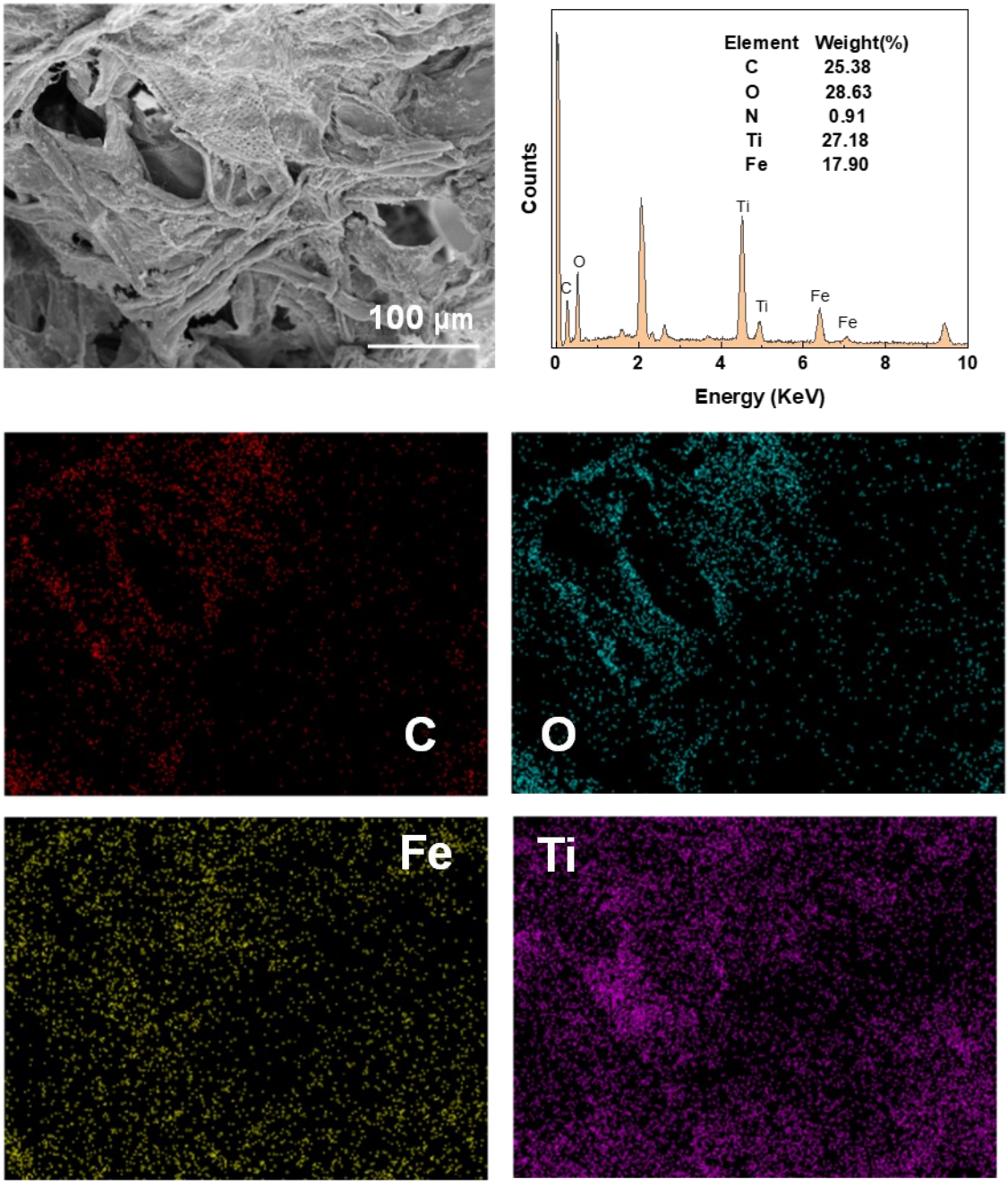

Fig. 4. SEM images and EDS data of AP-BC/TiO_2 magnetic aerogel

The highly open and oriented multichannel network provides abundant accessible active sites, shortens mass-transfer pathways, and accelerates the diffusion of adsorbate molecules into the internal structure. The uniformly dispersed Fe_3O_4 and TiO_2 nanoparticles on pore walls further increase surface roughness and specific surface area (Hemdan *et al.*, 2025), strengthening electrostatic attraction and surface complexation with target pollutants (El-Sawaf *et al.* 2024b). Consequently, the well-developed porous morphology and homogeneous particle distribution synergistically boost adsorption capacity, removal efficiency, and structural stability of the aerogel (Adaileh *et al.* 2025).

Magnetic performance analysis

The magnetic hysteresis loops of AP-BC/TiO_2 magnetic aerogels with different mass concentrations of TiO_2 are shown in Fig. 5. The magnetic aerogel with a TiO_2 mass concentration of 1 $g \cdot L^{-1}$ exhibited a weak ferromagnetic property with saturation magnetization (Ms) of 17.24 $emu \cdot g^{-1}$, which is consistent with the SEM-EDS results. As the mass concentration of TiO_2 increased, a trend of first increasing and then decreasing was observed. Overall, it can be manipulated using a magnet (Figs. 5b, c), and its magnetism can be completely recycled and reused, fulfilling the experimental criteria.

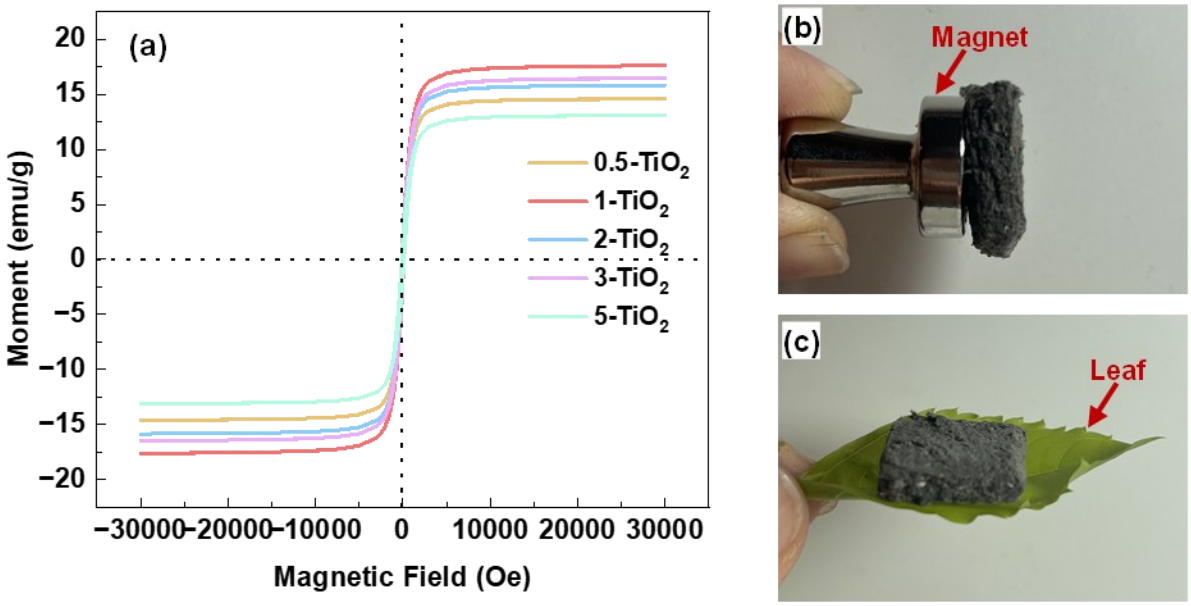

Fig. 5. The magnetic hysteresis loops of AP-BC/TiO_2 magnetic aerogels with different mass concentration concentrations of TiO_2(a), magnetic adsorption(b),and appearance (c),of AP-BC/TiO_2 magnetic aerogels

CONCLUSIONS

1. A novel ternary deep eutectic solvent (DES) ($ZnCl_2$/H_3PO_4/$NH_4H_2PO_4$) allowed for room-temperature extraction of bagasse cellulose, realizing selective removal of impurities, preserving high crystallinity (54.8%), and laying a structural foundation for subsequent modification.
2. Optimized mild sequential modification enabled successful grafting of dual functional groups, preventing excessive crystalline damage to cellulose.
3. Atmospheric pressure foaming was utilized instead of energy-intensive freeze-drying for aerogel fabrication, integrating adsorption–photocatalysis–magnetic separation and yielding a saturation magnetization of 17.2 $emu \cdot g^{-1}$.
4. Box-Behnken design – Response Surface Modeling (BBD-RSM) was used to optimizes four key parameters ($R^2 = 0.9747$), achieving an exceptional MB adsorption capacity of 1070 $mg \cdot g^{-1}$ and surpassing the unmodified sample (209 $mg \cdot g^{-1}$). The results demonstrate high adsorption efficiency.

5. This study not only realizes the high-value utilization of sugarcane bagasse and the green preparation of aerogels but also provides an innovative paradigm for designing multi-functional, high-performance biomass-based adsorbents, aligning with the principles of circular economy and sustainable development.

ACKNOWLEDGMENTS

The authors are grateful for the support of Guangxi Natural Science Foundation Joint Special Project (Grant No.2026GXNSFHA00640025), the Young Scientists Fund of Guangxi Natural Science Foundation (Grant No. 2023GXNSFBA026289), Wuzhou Science and Technology Plan Project (Research on Synergistic Removal of Binary Pollutants in Water by Magnetic Biomass Aerogels, Grant No. 202402027), the Key Support Project (Emerging Engineering Education) of the National College Students' Innovation and Entrepreneurship Training Program (Preparation and Photocatalytic Performance of Bagasse-based Magnetic Aerogels, Grant No. 202411354024), Special Project for Young Innovative Talents in Project of Guangxi Science and Technology Base and Special Talent (Grant No. Guike AD22080018), Doctoral Foundation of Scientific Research Project of Wuzhou University (Green Construction and Electrochemical Performance of Carbon Film based on Chinese Medicine Residue, Grant No. 2022A001), Key Project of Wuzhou University (Design and Supercapacitive Performance of Biomass-Derived Carbon Materials/MXene Flexible Films, Grant No. 2024ZD005), and Education and Teaching Reform Project of Wuzhou University (Exploration and Practice of "Craftsman-type" Talent Training Mode in Applied Undergraduate Universities from the Perspective of Emerging Engineering Education, Grant No. Wyjg2023A053).

Use of Generative AI

Douba AI was used for literature organization in the introduction section, and MogoEdit (https://www.mogoedit.com) was used for its English editing during the preparation of this manuscript.

REFERENCES CITED

Adaileh, A. D., Ragab, A. H., Taher, M. A., Gumaah, N. F., Soliman, M. S., Taha, A., and Mubarak, M. F. (2025). "Development of a double-shelled nanocomposite of activated carbon-nanocellulose with cationic metal oxide core for enhanced adsorption of bicarbonate from underground water," *Inorganic Chemistry Communications* 173, article 113779. https://doi.org/10.1016/j.inoche.2024.113779

Almeida, R. O., Maloney, T. C., and Gamelas, J. A. F. (2023). "Production of functionalized nanocelluloses from different sources using deep eutectic solvents and their applications," *Industrial Crops and Products* 199, article 116583. https://doi.org/10.1016/j.indcrop.2023.116583

Alslaibi, T. M., Abustan, I., Ahmad, M. A., and Foul, A. A. (2013). "Cadmium removal from aqueous solution using microwaved olive stone activated carbon," *J. Environ. Chem. Eng.* 1(3), 589-599. https://doi.org/10.1016/j.jece.2013.06.028

Chen, L., Yu, X., Gao, M., Xu, C., Zhang, J., Zhang, X., Zhu, M., and Cheng, Y. (2024). "Renewable biomass-based aerogels: From structural design to functional

regulation," *Chemical Society Reviews* 53(14), 7489-7530. https://doi.org/10.1039/d3cs01014g

Chen, M., Zhang, X., Zhang, A., Liu, C., and Sun, R. (2016). "Direct preparation of green and renewable aerogel materials from crude bagasse," *Cellulose* 23(2), 1325-1334. https://doi.org/10.1007/s10570-015-0814-9

Dai, H., Chen, Y., Ma, L., Zhang, Y., and Cui, B. (2021). "Direct regeneration of hydrogels based on lemon peel and its isolated microcrystalline cellulose: Characterization and application for methylene blue adsorption," *International Journal of Biological Macromolecules* 191, 129-138. https://doi.org/10.1016/j.ijbiomac.2021.09.063

Elfiky, A. A. E. A., Mubarak, M. F., Keshawy, M., Sayed, I. E. T. E., and Moghny, T. A. (2024). "Novel nanofiltration membrane modified by metal oxide nanocomposite for dyes removal from wastewater," *Environment, Development and Sustainability* 26(8), 19935-19957. https://doi.org/10.1007/s10668-023-03444-1

El-Sawaf, A. K., El-Dakkony, S. R., Zayed, M. A., Eldesoky, A. M., Nassar, A. A., El Shahawy, A., and Mubarak, M. F. (2024a). "Green synthesis and characterization of magnetic gamma alumina nanoparticlesfor copper ions adsorption from synthetic wastewater," *Results in Engineering* 22, article 101971. https://doi.org/10.1016/j.rineng.2024.101971

El-Sawaf, A. K., Nassar, A. A., El Aziz Elfiky, A. A., and Mubarak, M. F. (2024b). "Advanced microcrystalline nanocellulose-based nanofiltration membranes for the efficient treatment of wastewater contaminated with cationic dyes," *Polymer Bulletin* 81(14), 12451-12476. https://doi.org/10.1007/s00289-024-05279-w

Fang, H., Shan, B., Han, C., Zhu, B., Gu, C., Tan, W., Tian, Y., Ma, J., and Liu, T. (2025). "Recent progress in core-shell composites for adsorption in wastewater treatment," *Separation and Purification Technology* 2025, article 135480. https://doi.org/10.1016/j.seppur.2025.135480

Fu, F. and Wang, Q. (2011). "Removal of heavy metal ions from wastewaters: A review," *Journal of environmental management* 92(3), 407-418. https://doi.org/10.1016/j.jenvman.2010.11.011

Gong, W., Liu, M., Hu, B., Fan, L., Ye, D., and Xu, J. (2025). "Room-temperature and recyclable preparation of cellulose nanofibers using deep eutectic solvents for multifunctional sensor applications," *International Journal of Biological Macromolecules* 296, article 139739. https://doi.org/10.1016/j.ijbiomac.2025.139739

Gupta, V. K., Kumar, R., Nayak, A., Saleh, T. A., and Barakat, M. A. (2013). "Adsorptive removal of dyes from aqueous solution onto carbon nanotubes: A review," *Advances in Colloid and Interface Science* 193, 24-34. https://doi.org/10.1016/j.cis.2013.03.003

Hemdan, M., Ragab, A. H., Elyan, S. S., Taher, M. A., and Mubarak, M. F. (2025). "Eco-friendly activated carbon thin film-zeolitic imidazolate framework-8 (ACTF@ ZIF-8) nanocomposite for efficient methylene blue removal: Synthesis, characterization, and adsorption performance," *Journal of Cluster Science* 36(1), 2. https://doi.org/10.1007/s10876-024-02730-w

Hubbe, M. A., Azizian, S., and Douven, S. (2019). "Implications of apparent pseudo-second-order adsorption kinetics onto cellulosic materials. A review," *BioResources* 14(3), 7582-7626. https://doi.org/10.15376/biores.14.3.7582-7626

Liu, W., Dai, C., He, L., Liu, X., Zhao, Z., Yan, W., Yuan, M., Song, Z., and Cui, S. (2025). "Biomass aerogel: An emerging eco-friendly material for adsorbing pollutants

in water," *Chemical Engineering Journal* 2025, article 162977. https://doi.org/10.1016/j.cej.2025.162977

Mubarak, M. F., Selim, H., Hawash, H. B., and Hemdan, M. (2024). "Flexible, durable, and anti-fouling maghemite copper oxide nanocomposite-based membrane with ultra-high flux and efficiency for oil-in-water emulsions separation," *Environmental Science and Pollution Research* 31(2), 2297-2313. https://doi.org/10.1007/s11356-023-31240-x

Muthukumar, M., Mohan, D., and Rajendran, M. (2003). "Optimization of mix proportions of mineral aggregates using Box Behnken design of experiments," *Cement Concrete Comp* 25(7), 751-758. https://doi.org/10.1016/S0958-9465(02)00116-6

Nassar, A. A., Mubarak, M. F., El-Sawaf, A. K., Zayed, M. A., and Hemdan, M. (2025). "Efficient lead ion removal from aqueous solutions for wastewater treatment using a novel cross-linked alginate-rice husk ash-graphene oxide-chitosan nanocomposite," *International Journal of Biological Macromolecules* 284, article 137983. https://doi.org/10.1016/j.ijbiomac.2024.137983

Nie, Y., Zhou, Y., Zhang, Y., Sun, D., Wu, D., Ban, L., Nanda, S., Xu, C., and Zhang, H. (2025). "Sustainable synthesis of functional materials assisted by deep eutectic solvents for biomedical, environmental, and energy applications," *Advanced Functional Materials* 35(19), article 2418957. https://doi.org/10.1002/adfm.202418957

Nuopponen, M., Vuorinen, T., Jämsä, S., and Viitaniemi, P. (2005). "Thermal modifications in softwood studied by FT-IR and UV resonance Raman spectroscopies," *Journal of Wood Chemistry and Technology* 24(1), 13-26. https://doi.org/10.1081/WCT-120035941

Qiu, C., Tang, Q., Zhang, X., Li, M.-C., Zhang, X., Xie, J., Zhang, S., Su, Z., Qi, J., Xiao, H., et al. (2022). "High-efficient double-cross-linked biohybrid aerogel biosorbent prepared from waste bamboo paper and chitosan for wastewater purification," *Journal of Cleaner Production* 338, article 130550. https://doi.org/10.1016/j.jclepro.2022.130550

Ragab, A. H., Gumaah, N. F., El Aziz Elfiky, A. A., and Mubarak, M. F. (2024a). "Exploring the sustainable elimination of dye using cellulose nanofibrils-vinyl resin based nanofiltration membranes," *BMC Chemistry* 18(1), article 121. https://doi.org/10.1186/s13065-024-01211-5

Ragab, A. H., Mettwally, B. S., Mubarak, M. F., Al-Ghamdi, A., and Hemdan, M. (2024b). "Eco-friendly electrospinning of recycled nylon 6, 12 waste for high-performance nonwoven nanofibers in sustainable textile applications," *Journal of Inorganic and Organometallic Polymers and Materials* 34(4), 1491-1505. https://doi.org/10.1007/s10904-023-02851-1

Ramzi, M., Hosny, R., El-Sayed, M., Fathy, M., and Moghny, T. A. (2016). "Evaluation of scale inhibitors performance under simulated flowing field conditions using dynamic tube blocking test," *Int. J. Chem. Sci* 14(1), 16-28.

Salem, K. S., Kasera, N. K., Rahman, M. A., Jameel, H., Habibi, Y., Eichhorn, S. J., French, A. D., Pal, L., and Lucia, L. A. (2023). "Comparison and assessment of methods for cellulose crystallinity determination," *Chemical Society Reviews* 52(18), 6417-6446. https://doi.org/10.1039/d2cs00569g

Segal, L., Creely, J. J., Martin, A. E., and Conrad, C. M. (1959). "An empirical method for estimating the degree of crystallinity of native cellulose using the x-ray diffractometer," *Text. Res. J.* 29(10), 786-794. https://doi.org/10.1177/004051755902901003

Sen, S., Singh, A., Bera, C., Roy, S., and Kailasam, K. (2022). "Recent developments in biomass derived cellulose aerogel materials for thermal insulation application: A review," *Cellulose* 29(9), 4805-4833. https://doi.org/10.1007/s10570-022-04586-7

Su, H., Qiu, W., Hu, T., Peng, K., Liu, W., Chen, G., Zhao, Y., Xu, Z., Wang, H., and Wen, P. (2024). "Biobased amphoteric aerogel with core-shell structure for the hierarchically efficient adsorption of anionic and cationic dyes," *Journal of Hazardous Materials* 480, article 136235. https://doi.org/10.1016/j.jhazmat.2024.136235

Tong, Z., Liu, S., Tang, H., Liu, J., Bi, W., Liu, Y., Zeng, S., Xia, Q., Zhao, D., and Yu, H. (2025). "Super-robust cellulose rayon filaments engineered via molecular orientation-cross-linking assembly," *Nano Letters* 25(39), 14489-14496. https://doi.org/10.1021/acs.nanolett.5c04065

Xiao, W., Sun, R., Hu, S., Meng, C., Xie, B., Yi, M., and Wu, Y. (2023). "Recent advances and future perspective on lignocellulose-based materials as adsorbents in diverse water treatment applications," *International Journal of Biological Macromolecules* 253, article 126984. https://doi.org/10.1016/j.ijbiomac.2023.126984

Xiong, J., Zhang, D., Lin, H., and Chen, Y. (2020). "Amphiprotic cellulose mediated graphene oxide magnetic aerogels for water remediation," *Chemical Engineering Journal* 400, article 125890. https://doi.org/10.1016/j.cej.2020.125890

Yuan, Y., Li, S., Jiao, F., Shen, G., Yan, L., and Wang, W. (2019). "Dimensional stability improvement of corn stalk biocomposites using two-part lignin-derived binder optimized with response surface methodology," *BioResources* 14(3), 5923-5942. https://doi.org/10.15376/biores.14.3.5923-5942

Zeng, X., Zhu, J., Zhang, G., Wu, Z., Lu, J., and Ji, H. (2023). "Molecular-level understanding on complexation-adsorption-degradation during the simultaneous removal of aqueous binary pollutants by magnetic composite aerogels," *Chemical Engineering Journal* 468, article 143536. https://doi.org/10.1016/j.cej.2023.143536

Article submitted: February 17, 2026; Peer review completed: April 22, 2026; Revised version received: July 18, 2026; Accepted: August 3, 2026; Published: August 14, 2026.
DOI: 10.15376/biores.21.4.9730-9746